Long-Lived Intracellular Single-Molecule Fluorescence Using Electroporated Molecules

Robert Crawford, Joseph P. Torella, Louise Aigrain, Anne Plochowietz, Kristofer Gryte, Stephan Uphoff, and Achillefs N. Kapanidis*
Biological Physics Research Group, Clarendon Laboratory, Department of Physics, University of Oxford, Oxford, United Kingdom

ABSTRACT   Studies of biomolecules in vivo are crucial to understand their function in a natural, biological context. One powerful approach involves fusing molecules of interest to fluorescent proteins to study their expression, localization, and action; however, the scope of such studies would be increased considerably by using organic fluorophores, which are smaller and more photostable than their fluorescent protein counterparts. Here, we describe a straightforward, versatile, and high-throughput method to internalize DNA fragments and proteins labeled with organic fluorophores into live *Escherichia coli* by employing electroporation. We studied the copy numbers, diffusion profiles, and structure of internalized molecules at the single-molecule level in vivo, and were able to extend single-molecule observation times by two orders of magnitude compared to green fluorescent protein, allowing continuous monitoring of molecular processes occurring from seconds to minutes. We also exploited the desirable properties of organic fluorophores to perform single-molecule Förster resonance energy transfer measurements in the cytoplasm of live bacteria, both for DNA and proteins. Finally, we demonstrate internalization of labeled proteins and DNA into yeast *Saccharomyces cerevisiae*, a model eukaryotic system. Our method should broaden the range of biological questions addressable in microbes by single-molecule fluorescence.

INTRODUCTION

Single-molecule detection has transformed our perspective on biological mechanisms and systems, based largely on fluorescence methods such as fluorophore counting and tracking (1–3), single-molecule Förster resonance energy transfer (4) (smFRET) and localization-based super-resolution imaging (5–8). Single-molecule fluorescence is increasingly employed inside living cells (9–15), addressing interactions between fluorescent molecules of interest and cellular factors such as macromolecular crowding, gene expression stochasticity, redox status, the presence of cytoplasmic components, and localization to cell compartments.

Most fluorescence studies inside living cells depend on protein fusions with green fluorescent protein (GFP) and its variants (16) (fluorescent proteins or FPs). FP-based methods can monitor the copy number, diffusion pattern, or localization of proteins in processes such as gene expression and membrane transport (10,12,13,17–19). Similar methods have allowed high-resolution imaging of subcellular structures (20). FPs can also be used to study RNA (e.g., using MS2-GFP (21)) and DNA (e.g., using DNA-binding proteins (20)). The popularity of FPs is due in part to the ease and specificity of protein labeling and the large inventory of FP variants with various photophysical and chemical properties (16).

Although FP fusions are a powerful tool, there are applications for which FPs are less well suited than their organic fluorophore counterparts. First, FPs are significantly less photostable (up to 100-fold) than organic fluorophores typically used for in vitro applications (22,23). Due to their higher photon budget, organic fluorophores offer increased localization precision and slower photobleaching, and can be preferable in super-resolution imaging and single-molecule tracking. Second, due to the large size of FPs (~100-fold larger volume than organic dyes), the restricted rotation of the FP fluorophore, and the complexity of intramolecular labeling, FPs are seldom used as FRET pairs in vivo (24) or at the single-molecule level. Inserting two FPs into a protein or protein complex may also interfere with the structure or interaction studied, or cause artifactual protein-protein interactions (25). Some limitations may be overcome by intracellular labeling of proteins fused to polypeptide tags (e.g., SNAP, HALO, or TMP tags) (26–29), but this still requires large protein fusions (e.g., SNAP tag: 20 kDa). Finally, unnatural amino acid labeling is a very promising avenue but their implementation still remains a challenging procedure (30).

Another path to site-specifically label proteins in vivo involves delivery of in vitro organic dye-labeled proteins into living cells. Methods to internalize molecules into living cells such as scrape loading, syringe loading, and microinjection (31–33) are attractive, but applicable only to large, single-membrane eukaryotic cells. Along these lines, Sakon and Weninger used microinjection of labeled proteins into live mammalian cells (34), enabling in vivo smFRET measurements. However, microinjection is not an option for microbes, as the needle diameter is too large for most

---

microbial cells (e.g., *Escherichia coli* ~2–4 *μ*m long; needle diameter ~1 *μ*m wide (34)); cell walls are also barriers to microinjection even in organisms large enough to tolerate a needle (35). Moreover, as only one cell can be microinjected at a time, studies of cell-to-cell variation using this approach may be a laborious task. Finally, methods such as heat shock, electroporation, sonoporation, and detergent treatment (36–38) have been used to internalize DNA into microorganisms and could in principle load labeled molecules into cells, but have not been characterized for such a purpose.

Here, we describe a general, high-throughput method to internalize and observe single fluorescent biomolecules in microorganisms by adapting electroporation (37,38) and combining it with fluorescence imaging. Electroporation, typically used for cell transformation with plasmid DNA, relies on discharging a high-voltage electric field across a low ionic strength cell suspension to form transient membrane pores through which biomolecules can enter cells (Fig. 1 *A*). We used electroporation to internalize fluorescently labeled DNA and proteins of sizes up to 100 kDa into *E. coli*. Individual molecules labeled with organic fluorophores could be tracked with high temporal resolution for timescales an order of magnitude longer than FPs (3,34). We observed smFRET in live bacteria using both DNAs and proteins. Our methods are compatible with widefield (WF), total internal reflection fluorescence (TIRF), and confocal detection, as well as alternating laser excitation (ALEX) (39,40). We also show successful electroporation-based DNA and protein internalization into the yeast *Saccharomyces cerevisiae*, demonstrating the applicability of our technique to genetically diverse microorganisms.

MATERIALS AND METHODS

Preparation of DNAs

Oligonucleotides were prepared by automated synthesis (IBA GmbH). The sequences used are shown below; the underlined T base was labeled either with Cy3B (STD45T) or ATTO647N (STD45B series) or Alexa647. *STD45T*: 5′T̲AAATCTAAA GTAACATAAGGTAACATAACGTAAGCTC ATTCGCG-3′; *STD45B dT13*: 5′-CGCGAA TGAGCT̲T̲ACGTTATGTTA CCTTATGTTACTTTAGATTTA-3′; *STD45B dT28*: 5′-CGCGAATGAGCT TACGTTATGTTACCT̲T̲ATGTTACTTTAGATTTA-3′; *STD45B dT38*: 5′-CG CGAATGAGCTTACGTTATGTTACCTTATGTTACTT̲T̲AGATTTA-3′

Labeling at the 5′-end of oligonucleotides was performed using the 5′-amino-C6-modifying group with a 10-fold excess of *N*-hydroxy-succinimidyl esters of Cy3B (GE Healthcare) or ATTO647N (ATTO-TEC) using manufacturer's instructions, and were PAGE-purified. Internal labeling was performed using the same protocol, but using a 20-fold excess of dye. Low-, intermediate-, and high-FRET double-stranded DNA (dsDNA) standards were prepared by annealing labeled versions of STD45T (top strand) to either STD45B dT13, STD45B dT28, or STD45B dT38, respectively (bottom strands). Oligos were annealed in low-salt annealing buffer (20 mM Tris-HCl (pH 8.0), 50 mM NaCl, 1 mM EDTA) by heating to 94°C and subsequent cooling to 4°C over 45 min in steps of 10°C.

Labeled protein preparation

Catabolite activator protein (CAP) (Cys-17, Ser-178) was site-specifically labeled as described (41). Labeling was performed by adding a threefold excess of Alexa647 maleimide (Life Technologies) to the protein in a labeling buffer containing 40 mM HEPES pH 7.4, 0.2 mM cAMP, 200 mM KCl, 1 mM EDTA, and 0.1 mM TCEP. After an overnight incubation at 4°C, the reaction was quenched by the addition of 10 mM DTT for 30 min at 25°C. Products were purified using a Toyopearl HW-50 gel filtration column (Tosoh Bioscience) and stored at −20°C in a buffer containing 40 mM Tris-HCl pH8, 400 mM KCl, 1 mM EDTA, and 20% glycerol. The extent of labeling, calculated using UV-Vis spectroscopy and SDS-PAGE was >90%. Labeled CAP activity was determined by electrophoretic mobility shift assay to be ~30%.
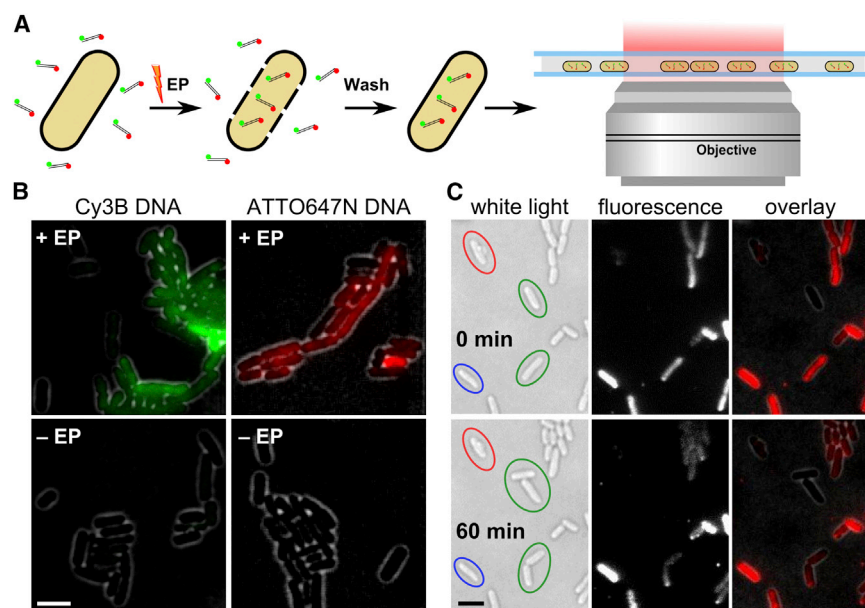

FIGURE 1 Electroporation of fluorescent DNA into living bacteria. (*A*) Schematic of internalization and observation methods. Fluorescent molecules are incubated with electrocompetent *E. coli* before electroporation. Cells are recovered, washed, and placed on agarose pads for imaging. (*B*) Overlay of inverted WL and fluorescence images of *E. coli* electroporated with 10 pmol dsDNA labeled with a green (Cy3B, *left*) or red (ATTO647N, *right*) fluorophore. +EP (*top*): electroporated cells, most with significant fluorescence. −EP (*bottom*): nonelectroporated cells, with negligible fluorescence. (*C*) Cell viability after electroporation at 1.8 kV/cm field strength. WL (*left*), fluorescence (*middle*), and overlay (*right*) of cells electroporated with 100 pmol AT-TO647N-labeled dsDNA at 0 and 60 min after recovery, deposited on coverslips, and grown in rich media at 37°C while observed using WF fluorescence imaging. Approximately 50% of electroporated cells (182 out of 362) divide within 60 min (e.g., *green ovals*), ~45% do not divide (e.g., *blue oval*), and <5% lose their integrity as judged by changes in their shape in the WL image (e.g., *red oval*). Cell viability is independent of cell loading. Scale bars: 3 *μ*m.

DNA Pol I Klenow fragment (KF) was prepared as described (42). Labeled proteins were stored at $-20°C$ in 50 mM Tris-HCl, pH 7.5, 1 mM DTT, and 40% glycerol. The extent of labeling, calculated from the UV-Vis spectrum, was $\geq 70\%$.

Electrocompetent cells

The commercial electrocompetent bacterial cell line used for electroporation was ElectroMAX DH5α-E Competent Cells (Invitrogen). Cells were diluted 1:1 with sterile milli-Q water and stored at $-80°C$. 20 μl cells were used for each electroporation experiment. Electrocompetent *S. cerevisiae* cells were prepared before each electroporation experiment. A 50 ml YPD medium culture was shaken at $30°C$ until it reached an OD_{600nm} of 0.8. Cells were harvested by spinning at 5000 rpm for 5 min at $4°C$ and the pellet was resuspended in 25 ml cold water. The washing procedure was repeated twice with 25 ml cold water and twice with 2 ml 1 M cold sorbitol. Finally, cells were resuspended in 250 μl 1 M sorbitol and split into 50 μl aliquots.

Electroporation

Up to 5 μl of labeled molecules stored in a low-salt buffer were added to the competent cells (20 or 50 μl aliquots for bacterial or yeast cells, respectively) and incubated 10 min on ice. The mixture of competent cells and labeled molecules was transferred into a prechilled electroporation cuvette (0.1 cm or 0.2 cm gap cuvette from Bio-Rad for bacteria or yeast electroporation, respectively) and placed into an electroporator (MicroPulser, Bio-Rad). An electric field of 1.8kV/cm was applied for bacteria electroporation and 1.5 kV/cm for yeast. 1 mL of super optimal broth with catabolite repression (SOC) or YPD medium was added immediately after electroporation. Cells were allowed to recover for 2 to 30 min at 37 or $30°C$. After recovery, cells were harvested by centrifugation at $3300 \times g$ for 1 min at $4°C$ and washed 5 times with 500 μL phosphate buffered saline (PBS) in the case of DNA internalization. Cells were resuspended in 100 μl PBS and placed on agarose-M9 pads before imaging. The pads themselves were made from ~250 μL of M9 medium containing 1% (v:w) BioRad Certified Molecular Biology Agarose on a coverslip. After the cells were pipetted onto the pad, another coverslip was added on top. The slide/agar sandwich was inverted and placed on the microscope with the side containing the cells closest to the objective.

For protein internalization, the same washing steps were used, but with a washing buffer containing PBS, 0.005% Triton X100, and 100 mM NaCl; this washing procedure removes any noninternalized proteins that may stick to the external cell membrane. With this optimized protocol, negative controls (sample corresponding to cells to which labeled proteins are added but no electroporation is performed) exhibit a fluorescence level similar to empty cell autofluorescence and much lower than electroporated samples.

WF cell imaging

Single-cell and single-molecule fluorescence microscopy in live bacteria was performed on a customized inverted Olympus IX-71 microscope equipped with two lasers, a 638-nm diode laser (Cube; Coherent) and a 532-nm Nd:YAG laser (Samba; Cobolt AB). Laser light was combined into a single-mode optical fiber (Thorlabs) and collimated before focusing on the objective. Cells were imaged using either WF or near-TIRF (nTIRF; also known as HILO (43)) illumination by adjusting the position of the focused excitation light on the back focal plane of the objective. Typical excitation powers were 0.5–3 mW for WF and nTIRF illumination. Long single-molecule tracks (see Fig. 3 *A*) used higher excitation powers of 10–15 mW in WF illumination. Long time traces (see Fig. 3, *C* and *D*), and photobleaching times used excitation powers of 0.3–0.6 mW in nTIRF illumination. Exposure times ranged from 15 to 100 ms. Cellular fluorescence was collected through the same objective, filtered to remove excitation light through a long-pass filter (HQ545LP; Chroma) and a notch filter (NF02-633S; Semrock), and spectrally separated by a dichroic mirror (630DRLP, Omega). Each channel was imaged onto separate halves of the chip of an electron-multiplying charge-coupled device camera (iXon+, BI-887, Andor). The illumination for white light (WL) images comprised a WL lamp (IX2-ILL100; Olympus) and condenser (IX2-LWUCD; Olympus) attached to the microscope. Movies and images were recorded using manufacturer's software or Micromanager (valelab.ucsf.edu/~MM/MMwiki/).

Confocal cell spectroscopy

For confocal measurements in *E. coli*, green and red ALEX was used, with laser light focused to a diffraction-limited spot inside the cell cytoplasm. Fluorescence emission was collected by the same objective, separated from excitation light and spatially filtered through a 100-μm pinhole to reject out-of-focus light. Fluorescence emission was split into green and red using a dichroic beamsplitter and filters, and focused onto separate avalanche photodiodes to detect photons and their arrival times. Photon arrival times were recorded with a PC counting board (PCI-6602; National Instruments). Typical excitation powers used were 180 μW for green and 60 μW for red (measured in continuous-wave mode). For ALEX experiments, the individual laser beams were modulated either directly through a TTL pulse, or using an acoustooptical modulator (Isomet) with a period of 100 μs.

Photobleaching analysis

For cell-based photobleaching analysis, cells were segmented manually using a custom-written MATLAB (The MathWorks, Natick, MA) script or automatically (with manual adjustment) by adapting the MATLAB implementation Schnitzcells (44) for WL cell images. The overall cell intensity per cell area was calculated for each movie frame from which was subtracted the cell autofluorescence per cell area after photobleaching using a custom-written MATLAB script. Baseline-subtracted photobleaching time traces showing <10 quantized steps were fitted with a hidden Markov model (HMM). Previously, HMM was used to analyze multichromophore photobleaching time traces (45). HMM is a stochastic model that maps measured values to unobserved (or hidden) states. Here, the time trajectories were modeled as a sequence of up to 10 hidden states (different cell intensity levels) and transitions between these states (photobleaching event). The Viterbi algorithm (46) was used to determine the state sequence fitting the photobleaching time trace best. A MATLAB script implementing the algorithms (HMM and Viterbi analysis) presented by Rabiner (47) was run recursively; for each iteration only the state values of the last photobleaching step were kept and the data belonging to the last photobleaching step was removed. Each iteration allowed up to 10 states to be fit. Such a method took advantage of the exponential photobleaching kinetics: the last photobleaching step was likely to last significantly longer than previous steps, and thus fitting the last step was likely to have the greatest data support. For the step size estimate of the fitted steps, the absolute difference between consecutive intensity states was calculated taking fluorophore blinking into account. Only step sizes from 57 time traces with <6 steps recovered by the HMM algorithm were plotted in a step size histogram. The step size histogram was fitted with a single one-dimensional-Gaussian (free fit parameters: position1, width1, amplitude1) and the single-molecule unitary intensity was given as the fitted mean position of the Gaussian. A small population of multiple simultaneous bleaching events accounts for larger step sizes that lie outside the single Gaussian fit. However, multiple Gaussian fitting, as well as the incorporation of step size values recovered from all 70 time traces with <10 steps does not significantly change the value of the single-molecule unitary intensity. The normalized and baseline-subtracted initial cell intensities were divided by the unitary fluorophore intensity to obtain the estimated number of internalized molecules.

Single-molecule tracking and diffusion analysis

Custom-written MATLAB software was used to analyze single-molecule tracking and diffusion in live *E. coli* which was based on a method similar to that in (3); see also (48). Briefly, the point spread functions (PSF) in each movie frame were fitted by a two-dimensional (2D) elliptical Gaussian (free fit parameters: *x/y* position, *x/y* width, elliptical rotation angle, amplitude, background) using initial position guesses from applying a fixed localization-intensity threshold on the bandpass filtered fluorescence image (49). Single-molecule tracking was performed by adapting the MATLAB script based on a published algorithm (50). Localized PSFs were linked to a track if they appeared in consecutive frames within a window of 5–7 pixels (0.48–0.67 μm). To account for PSF disappearance due to blinking or a missed localization, we used a memory parameter of 1 frame. Long-lived single-molecule tracks were visualized within the cell outline and the integral of the fitted 2D elliptical Gaussian above the background level of the tracked molecules were plotted. For each track with a minimum of four steps, an apparent diffusion coefficient D* was calculated from the mean squared displacement. The apparent diffusion coefficients were plotted in a histogram, where a peak at zero corresponds to nondiffusing molecules. We note that the apparent diffusion coefficient was corrected for the localization standard deviation of 30 nm but does not equal an accurate microscopic diffusion coefficient, because the step sizes are constrained by cell confinement and motion blurring during frame exposure time (51). The diffusion analysis method was tested simulating 2D and three-dimensional Brownian motion in a confined rod-shaped area showing good agreement of experimental and simulated data (48). Similar corrections to the experimental data were performed as (48).

Single-cell FRET efficiencies

Fluorescence and WL cell images acquired from the camera were processed using custom-written MATLAB scripts. For single-cell FRET analysis, ~300 cells were manually segmented in both the donor and acceptor emission channels (upon donor excitation). The fluorescence value for each cell in each channel was taken as the average pixel intensity within the cell boundary. A background value for each channel was taken as the average pixel intensity from a blank area of the slide. Background-subtracted fluorescence intensities were then used to calculate FRET for each cell. FRET was calculated as background-subtracted acceptor intensity divided by total (acceptor + donor) background-subtracted intensity upon donor excitation.

In vivo smFRET analysis

Localized PSFs inside cells were manually identified from movies and analyzed using Fiji and MATLAB. Average pixel intensities of the PSFs for each frame in both donor and acceptor channels were calculated from a circle fixed around each PSF (~3 pixel radius). Background values per channel were calculated from the average of the same size circle in a blank area of the slide over all frames analyzed. Background-subtracted fluorescence values in the donor and acceptor channel (upon donor excitation) were used for the fluorescence and FRET time traces, as in the single-cell FRET case.

Fluorescence overlay images and movies

Fluorescence images (see Fig. 5 and Video S1 in the Supporting Material) are an overlay of the donor and acceptor fluorescence channels colored green and red, respectively. The donor channel undergoes an image transformation to match the acceptor channel; the transformation matrix is based on a calibration matrix using fluorescent beads.

In vitro ALEX data analysis

Single-molecule fluorescence bursts from in vitro smFRET confocal microscopy were analyzed in MATLAB as described (52). Briefly, information on

photon arrival times, excitation cycle, and detection channel, enables the calculation of fluorescence bursts (donor or acceptor) arising due to molecules traversing the confocal spot under either donor or acceptor excitation. FRET efficiency (uncorrected), E*, and relative probe stoichiometry, S, were calculated as follows:

$$E^* = \frac{F_{Dex}^{Aem}}{F_{Dex}^{Aem} + F_{Dex}^{Dem}} \text{ and } S = \frac{\left(F_{Dex}^{Aem} + F_{Dex}^{Dem}\right)}{\left(F_{Dex}^{Aem} + F_{Dex}^{Dem} + F_{Aex}^{Aem}\right)},$$

where F_{Xex}^{Yem} represents the fluorescence of a burst arising in the Y emission channel under X excitation.

RESULTS

Introducing fluorescent DNA into *E. coli* via electroporation

We first asked whether we could use electroporation to introduce a fluorescently labeled 45-bp dsDNA into live *E. coli*. A suspension of 20 μl electrocompetent *E. coli* DH5α cells was incubated with 10 pmol Cy3B-labeled dsDNA for 10 min, electroporated at an initial field strength of 1.8 kV/cm, and recovered for 20 min in rich media (Methods: techniques for DNA labeling and protein purification; electroporation; single-cell microscopy; and single-molecule fluorescence spectroscopy (along with bleaching, single-molecule tracking, and diffusion analysis) are all described in the Supporting Material text). Following washing, deposition on agar-coated coverslips, and imaging (Fig. 1 A), >80% of cells exhibited intense fluorescence (Fig. 1 B, *top left*). In contrast, cells incubated with the same DNA, but not electroporated, showed no significant fluorescence (Fig.1 B, *bottom left*). Similar results were obtained using DNAs labeled with fluorophores exhibiting different structures and emission wavelengths (ATTO647N, Fig. 1 B, *right*; Alexa647, Fig. S1), suggesting that the choice of fluorophore is not crucial for successful electroporation. We also internalized dsDNA bearing FRET pairs and observed FRET in vivo (see section on smFRET), demonstrating that the internalized DNAs remain intact. These results suggested that short fluorescent DNAs can be efficiently electroporated into *E. coli*.

To assess the effect of electroporation and fluorescent DNA uptake on the ability of cells to grow and divide, we monitored the growth of cells electroporated with ATTO647N-labeled dsDNA at two different field strengths (0.9 and 1.8 kV/cm) on coverslips over several generations using WF imaging (Fig. 1 C). Lowering the field strength during electroporation increases cell viability, albeit with decreased internalization efficiency (Fig. S2 A). Maximal loading efficiency (~90%) was achieved at 1.8 kV/cm, wherein ~50% of electroporated cells divided within 1 h (*cells in green ovals*, Fig. 1 C), 45% did not grow but remained intact, and 5% appeared to have damaged membranes (Fig. 1 C, *cells in blue and red ovals*, respectively). For comparison, ~80% of nonelectroporated electrocompetent cells grew on the coverslip (Fig. S2 A). At 0.9 kV/cm,

loading efficiency remained above 70% (Fig. S2 A), whereas division frequencies were similar to those for nonelectroporated cells (78% vs. 84%). For dividing cells, the total fluorescence was preserved and distributed evenly between daughter cells (Fig. S2 B), and cell viability was independent of fluorescence load (Fig. 1 C), suggesting that the fluorescent DNAs are not toxic. These results showed that a large fraction of cells recover from electroporation, resume growth, and divide, and that internalization of fluorescent molecules does not hinder their recovery.
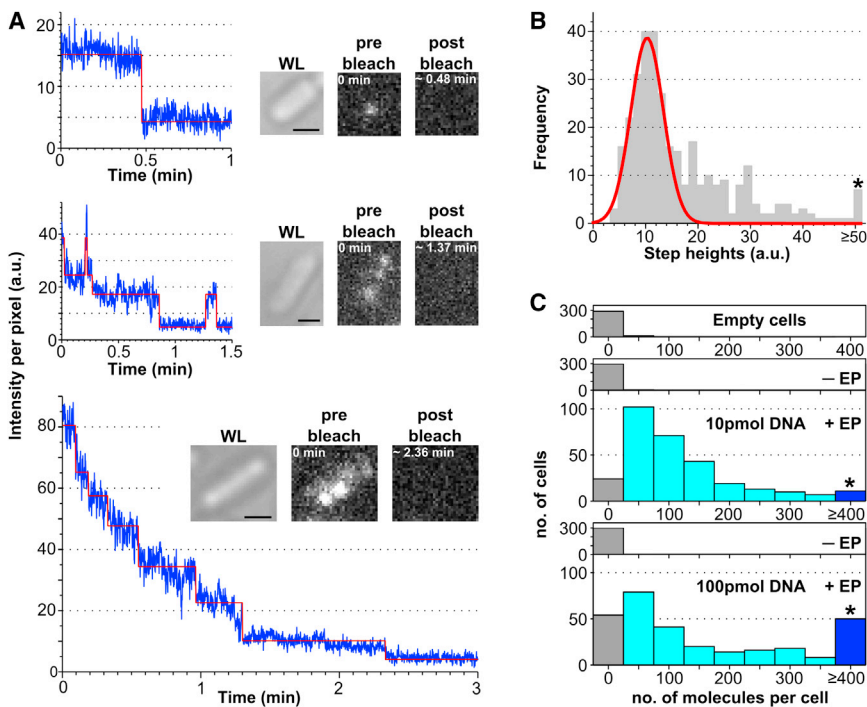
We next determined the number of molecules introduced into each cell. To do so, we illuminated cells continuously under WF conditions and, as they photobleached, measured the decrease in their average fluorescence intensity per pixel, f_p, a metric relatively immune to molecular diffusion in a cell. For cells with few fluorescent molecules ($N = 1$ to 3), f_p decreased over time in clear, fairly regular steps due to irreversible photodestruction of individual fluorophores (Fig. 2 A, top); long-lived dark states, a property associated with single fluorophores, were also observed (Fig. 2 A, middle). In both cases, individual fluorophores could be easily distinguished over cellular autofluorescence and persisted for up to minutes before bleaching. To measure the mean unitary fluorescence intensity per internalized fluorophore, we inspected 57 cells with $N < 6$ (Fig. 2 A, bottom) and performed stepwise photobleaching analysis using HMM (Methods); the step-size distribution, which included mostly single steps and a few double steps, yielded an estimate of ~8100 photons/s per step for the unitary fluorophore intensity (~11 $\pm$ 3 a.u., Fig. 2 B).

Division of average cellular fluorescence by the unitary intensity yields the number of fluorescent DNAs per cell. This value represents a lower estimate due to potential photophysical behavior of the dyes in vivo. Electroporating 10 pmol of fluorescent DNA led to >90% of cells showing fluorescence significantly higher than control cells (incubated with fluorescent DNA but not electroporated; Fig. 2 C). As expected from Fig. 1 B, there was a wide distribution in the numbers of internalized DNAs per cell, with a range of 10 to 500 molecules and a mean of ~120 molecules (std 106; median 87; Fig. 2 C, middle). Electroporation of 100 pmol of labeled DNA led to high internalization efficiency (>85%) and increased the mean number of internalized molecules to ~175 (std 187, median 91, range of N: 10–700; Fig. 2 C, bottom). Although the distribution of internalized molecules is not linear with added DNA concentration, this result shows that the mean number of internalized molecules can be adjusted by varying the amount of electroporated DNA.

Single-molecule tracking of internalized fluorescent DNA

Single-molecule tracking has allowed studies of protein mobility and interactions in cells; however, prolonged

FIGURE 2 Counting internalized molecules. (A) Single-cell bleaching analysis. Examples of fluorescence intensity time traces (blue: raw data; red: HMM fit; insets: WL and fluorescence images of E. coli loaded with ATTO647N-labeled dsDNA before and after bleaching). Top: single-step bleaching event. Middle: step analysis of cell containing ~3 molecules showing bleaching and blinking. Bottom: step analysis showing ~4 steps corresponding to diffusing molecules. (B) Histogram of single-step height intensities from HMM-fitted steps from 57 cells ($N < 6$) as in panel A. Single Gaussian fit is centered at 11 $\pm$ 3 a.u., corresponding to a unitary fluorophore intensity of 8100 photons per second (Methods). (C) Histogram of internalized molecules per cell electroporated with different amounts of ATTO647N dsDNA, calculated after dividing the initial fluorescence intensity by the unitary fluorophore intensity. Top to bottom: empty cells (i.e., nonincubated with fluorescent molecules and nonelectroporated), nonelectroporated (but incubated with fluorescent molecules), and electroporated cells incubated with 10 and 100 pmol dsDNA. Empty and nonelectroporated cells correspond to autofluorescence, whereas electroporated cells show a broad distribution of internalized molecules, with a higher proportion of highly loaded cells at 100 pmol (asterisk-marked bin). Internalization efficiency (defined as the fraction of cells showing higher fluorescence than the mean of the nonelectroporated sample plus three times the standard deviation of the nonelectroporated sample) for the 10 and 100 pmol samples: 94% and 90%, respectively. Mean number of internalized molecules per cell: 121 $\pm$ 106 molecules for 10 pmol dsDNA, and 176 $\pm$ 187 molecules for 100 pmol dsDNA. Settings: 100 ms exposure, WF illumination. Scale bars: 1 μm. To see this figure in color, go online.

tracking using FP fusions is challenging. We thus explored tracking of organic fluorophore-DNA conjugates in live *E. coli*. Following electroporation of *E. coli* with 2 pmol Cy3B-labeled DNA, we identified cells with few fluorescent DNA molecules ($N < 5$), and monitored them over time using WF illumination. Aided by the Cy3B brightness and photostability, we performed extended, continuous, high-precision single-molecule tracking (3,53,54) in vivo for >6 s with ~20 nm (*theoretical*, Thompson formula (53)) to 40 nm (*experimental*) localization precision (Fig. 3 *A*). Here, diffraction-limited images of single-fluorophores described by a PSF were fitted in each frame by a 2D elliptical Gaussian and then linked together to form tracks if they appeared within a predefined radius in consecutive frames. Such long tracks highlight diffusion paths in single cells and can identify changes in diffusion in vivo due to intermolecular interactions (48).

To obtain an apparent diffusion coefficient (D*) for Cy3B-labeled DNA, we analyzed the mean squared displacement of many short tracks (typically <0.5 s; Fig. 3 *B*, *left*) using nTIRF illumination (a.k.a. HILO (43)) and recovered a mean D* of ~0.92 μm^2/s. Tracking internalized Alexa647-labeled DNA molecules (Fig. 3 *A*, *bottom*) yielded a similar D* distribution (mean D* ~0.76 μm^2/s; Fig. 3 *B*, *right*), suggesting that the observed diffusion profile reflects the properties of DNA rather than the two fluo-

rophores used. We also studied the diffusion of DNA labeled with ATTO647N (one of the most photostable fluorophores); despite showing slightly slower diffusion than its Cy3B counterpart (mean D* ~0.61 μm^2/s; Fig. S3 *B*), the use of ATTO647N offered the longest tracks from all three fluorophores. Certain dyes such as ATTO647N can exhibit hydrophobic properties (55), which may affect diffusion behavior; therefore, careful selection of dyes may be important for particular applications.

We note that, due to effects from cell confinement and motion blurring, D* is just a lower bound for the actual diffusion coefficient, which is expected to be two- to threefold higher (3,48). The obtained estimate is ~10-fold slower than the diffusion coefficient measured in aqueous buffer (~40 μm^2/s). Slower diffusion in vivo (also seen for GFP (56–58)) is expected due to the highly viscous and crowded cytoplasm; DNA diffusion may also be slowed due to interactions with endogenous biomolecules.

To monitor molecules for longer times, we reduced the laser power 10-fold while increasing the exposure time, extending bleaching lifetimes from ~10 s to 1.8 min (Fig. 3 *C*, *inset*). These conditions allowed observations of up to 25 min for immobile or slowly diffusing molecules under continuous illumination (Fig. 3 *D*, Fig. S3 *C*) and are well suited for observing transient binding of molecules to
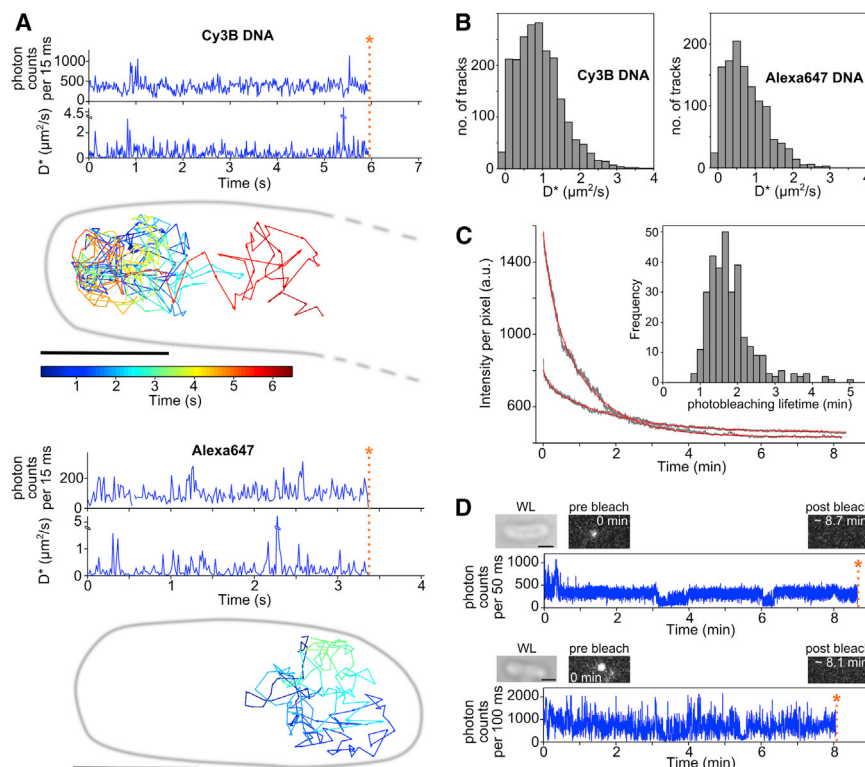

FIGURE 3 Single-molecule tracking of electroporated DNA in live bacteria. (*A*) Time traces and trajectories of internalized Cy3B-labeled DNA (*top*) and Alexa647-labeled DNA (*bottom*). Single-molecule photon-count time traces represent the PSF integrals fitted with 2D elliptical Gaussian above background level (*blue*). Tracks end due to dye bleaching (*orange line*, *asterisk*) as no PSF can be fitted by localization algorithm. Apparent diffusion coefficient time traces (*blue*; from squared displacements of each step) show fluctuations mainly due to diffusion. Time-colored trajectories show long tracks of single molecules exploring the cell volume (*gray boundary*). Settings: 15 ms exposure, WF illumination. All scale bars: 1 μm. (*B*) Apparent diffusion coefficient histogram for Cy3B-labeled DNA (*left*; 2117 tracks, 30 cells, mean D* ~0.92 μm^2/s, std: 0.61 μm^2/s) and Alexa647-labeled DNA (*right*; 1214 tracks, 60 cells, mean D* ~0.76 μm^2/s, std: 0.55 μm^2/s) calculated from mean squared displacement of each track. Settings: 10 ms exposure, nTIRF illumination. (*C*) Single-cell bleaching of internalized DNA labeled with ATTO647N. Main: Two examples of fluorescence time traces (*gray*). Photobleaching curves were fitted to a double exponential (*red*), with larger decay constant defined as the in vivo photobleaching lifetime. Inset: Histogram of photobleaching lifetimes from 309 cells, showing a mean of ~1.8 min.

Settings: 100 ms exposure, nTIRF illumination. (*D*) Observation of long-lived fluorescence from ATTO647N-labeled DNA. Examples of single-molecule time traces using 50-ms (*top*) and 100-ms (*bottom*) exposures for immobile or slowly diffusing molecules that last for up to 8 min. WL and fluorescence images of loaded cell before and after bleaching (nTIRF illumination). To see this figure in color, go online.

cellular structures or interacting molecules that diffuse slowly.

Electroporating labeled proteins into *E. coli*

The range of questions addressable in vivo would be greatly increased by electroporating organic fluorophore-labeled proteins (OFPs) into living bacteria. To deliver OFPs into cells and study the size dependence of protein delivery, we electroporated *E. coli* cells (Methods) with 10 pmol of Alexa647-labeled derivatives of two DNA binding proteins: the catabolic activator protein (CAP, 45 kDa; (59).) and the KF of DNA polymerase I (66 kDa; (60).) (Fig. 4, *A* and *B*). Both proteins were efficiently internalized, as most electroporated cells showed a clear red-fluorescent signal. Greater internalization efficiency (99%; Fig. 4 *A*) was observed for the smaller protein, CAP, whereas ~84% of cells were loaded with KF (Fig. 4 *B*). It is important to note that the numbers of fluorescent molecules counted per cell are likely to include a contribution from unattached free dye molecules present in the labeled protein sample as a contaminant. It is therefore crucial to remove as much of this contaminant as possible before electroporation, due to different internalization efficiencies between proteins and free dyes.

Using stepwise photobleaching analysis, we estimated a unitary fluorophore intensity of ~17 ± 4 a.u for both Alexa647-labeled KF and CAP. Initial fluorescence intensities per cell allowed us then to estimate that cells were loaded with up to ~600 fluorescent molecules for the CAP sample and ~200 molecules for the KF sample. Some CAP molecules appeared localized, consistent with CAP being a global regulator that can interact with >350 chromosomal sites upstream of promoters (61); on the other hand, cells loaded with KF show diffuse fluorescence, consistent with the diffusion profile observed for DNA polymerase I in *E. coli* (48). As with fluorescent DNA, the amount delivered depends on the amount of electroporated protein (Fig. S4).

To verify the presence and functionality of electroporated proteins in the cytoplasm, we electroporated unlabeled T7 RNA polymerase (98 kDa) into *E. coli* strain DH5α expressing the fluorescent protein EmGFP under the control of a T7 promoter. As the gene for T7 RNA polymerase is absent in DH5α, EmGFP expression requires that functional T7 RNA polymerase enters cells via electroporation (Fig. 4 *C*). Following electroporation with ~1 pmol T7 RNAP, ~11% of the cells (*blue bar*, Fig. 4 *C*) exhibited strong fluorescence higher than in the negative control (incubated with the same T7 RNAP amount, but not electroporated); the fraction of EmGFP-expressing cells should rise upon electroporating larger T7 RNAP amounts. This result established that a significant fraction of T7 RNAP molecules internalized by electroporation retain their
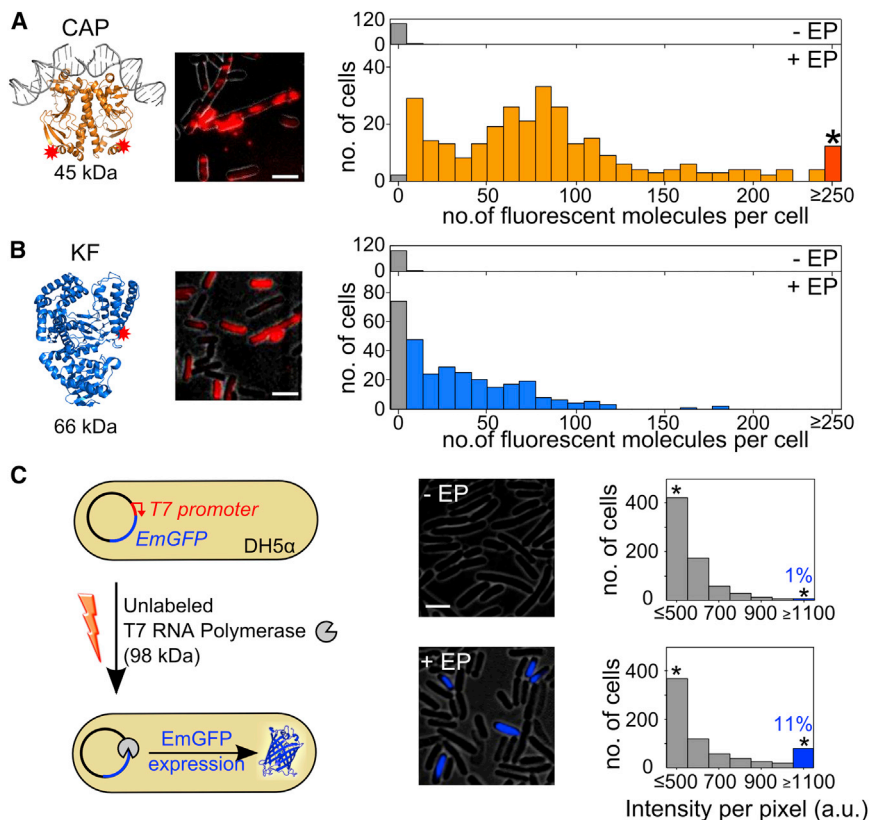

FIGURE 4 Protein internalization in live bacteria. (*A–B*) Cells electroporated with two Alexa647-labeled proteins: panel *A*, CAP (45 kDa) and panel *B*, KF of DNA polymerase I (KF, 66 kDa). Left: ribbon representation of the proteins (*orange* or *blue*) and DNA (*gray*). Labeling sites shown as red stars. Middle: fluorescence overlay of loaded cells. Right: Histogram of internalized fluorescent molecules per cell electroporated with 10 pmol protein. −/+ EP denotes incubation without/with electroporation. CAP and KF show up to ~99% and 84% internalization efficiency (defined as in Fig. 2 *C*). The number of internalized fluorescent molecules refers both to labeled proteins molecules and free dye molecules. Scale bars: 3 μm. (*C*) Internalization of unlabeled T7 RNA polymerase (T7 RNAP, 98 kDa) into electrocompetent DH5α carrying the pRSET-EmGFP plasmid encoding emerald GFP (EmGFP) under control of a T7 promoter. Left: Schematic of assay. Middle: fluorescence overlay. Right: histograms of cell-based fluorescence intensities for the nonelectroporated sample (*top*) and cells incubated and electroporated with T7 RNAP; ~11% of the electroporated cells show high fluorescence intensity (over our threshold corresponding to the mean fluorescence intensity of nonelectroporated cells plus three times the standard deviation). High fluorescence indicates expression of EmGFP. Scale bar: 3 μm.

integrity in vivo, and can perform their intended functions in the cell cytoplasm.

Internalizing doubly-labeled biomolecules for in vivo smFRET

As discussed, FP fusions are not ideal for smFRET. We therefore tested whether electroporation can deliver doubly-labeled biomolecules into *E. coli* to measure distances in the 1–10 nm scale inside living bacteria, enabling in vivo single-molecule studies of protein structure, interactions, and conformational dynamics. We thus electroporated cells with 20 pmol of three short doubly-labeled dsDNA FRET standards with apparent FRET efficiencies (E*) of 0.17, 0.48, and 0.86 in vitro (determined using ALEX spectroscopy; Fig. S5 A). All DNAs entered cells efficiently (Fig. 5 A, *left*), and the main peak of each single-cell E* distribution agreed well with the in vitro results (main peaks centered at E*~0.19, ~0.42, and ~0.75 for the low-, intermediate-, and high-FRET standards, respectively; Fig.5 A, *right*). In the intermediate- and high-FRET samples, there were also cell populations with lower E* than expected, presumably due to acceptor bleaching, variable cell loading (thus, variable signal/noise), and DNA degradation; the latter can be addressed by using DNAs with unnatural nucleic acids, or motifs that protect exonuclease-accessible termini. Our single-cell results suggested that, for all standards, most molecules remain intact over observation times of ~1 h.

To achieve in vivo smFRET, we electroporated small amounts (0.25 pmol) of intermediate- and high-FRET standards into *E. coli* (Fig. 5 B). Such concentrations led to many cells loaded with few (N = 1–10) labeled molecules, allowing direct localization, tracking, and FRET monitoring for single molecules. Some DNA molecules diffused freely, whereas others appeared immobile or diffused slowly (Movie S1). The presence of many near-diffraction-limited spots with high acceptor intensity upon donor excitation immediately suggested that many FRET pairs show a high FRET efficiency and thus are chemically and photophysically intact (Fig. 5, B and C, *left*; Movie S1). Time traces of immobilized intermediate-FRET DNA (Fig. 5 B, *middle*) lasted for 1 to 30 s and showed the hallmarks of smFRET: anticorrelated changes in the donor and acceptor fluorescence upon acceptor bleaching (t~16 s; Fig. 5 B, *middle*), followed by donor bleaching (t~19 s; Fig. 5 B, *middle*; see also Fig. S6). Using such traces, we generated an E* distribution (Fig. 5 B, *right*) with a mean value in excellent agreement to the in vitro results (0.45 in vivo; 0.48 in vitro). We obtained similar results for high-FRET DNA molecules (Fig. 5 C); the close agreement of the in vivo single-molecule E* value (0.77) with the in vitro value (0.86) confirmed our ability to distinguish intact molecules in the presence of bleaching or degradation. Representative in vivo single-molecule traces are

given in Fig. S6. The E* difference of ~0.09 between in vitro and in vivo values reflects differences in background (e.g., due to cellular autofluorescence), quantum yield (e.g., due to differences in global and localenvironment of the fluorophores), and cross talk factors between different experimental setups and detection geometries. Methods to account for such differences and calculate accurate smFRET efficiencies in vivo will involve procedures similar to the ones used in vitro (62), as well as comparisons that account for differences in the fluorophore environment (e.g., using GFP as a standard relative immune to the cellular environment).

We then performed similar measurements on a doubly-labeled KF protein derivative characterized in vitro (39,42), where it displayed millisecond-timescale dynamics between two structural states with E*~0.48 (open conformation) and ~0.66 (closed conformation); the 30-ms exposure time should yield a time-averaged E* of ~0.55. We first showed that KF exposure to high electrical fields does not affect the intramolecular FRET values measured in vitro (Fig. S5 B). We then electroporated *E. coli* cells with 5 pmol of doubly-labeled KF; as for DNAs, many electroporated cells were loaded with doubly-labeled KF molecules exhibiting efficient FRET. Most internalized proteins were diffusing rapidly (leading to diffuse fluorescence signals), whereas others were immobile for several seconds (Fig. 5 D, *left*). Time traces of immobile proteins (Fig. 5 D, *middle*, Fig. S6), as with DNA, showed the signatures of smFRET. The E* histogram for these traces (Fig. 5 D, *right*) was centered at E*~0.5, very close to the in vitro value. Intriguingly, the E* distribution for KF is wider than for intermediate-FRET DNA standards (Fig. 5 B), possibly reflecting the dynamic nature of KF, which adopts different conformations upon DNA and nucleotide binding (E* from ~0.4 to ~0.6 (39,42)). These results established our capability for quantitative smFRET studies on internalized proteins, and suggested these proteins can maintain their integrity and structure, further supporting our conclusions based on T7 RNAP internalization.

Confocal detection of internalized molecules

We also detected fluorescence and FRET from internalized DNA molecules in vivo using confocal optics and avalanche photodiodes, enabling 100-fold higher time resolution (~100 μs, Fig. S7). Upon focusing our laser into the cytoplasm of a cell, we detected fluorescence bursts due to the diffusion of internalized labeled DNAs through the confocal volume (Fig. S7). These bursts were absent in nonelectroporated cells, and exhibited a range of diffusion times (5–100 ms; Fig. S7, C and D); as the same DNAs exhibit diffusion times of ~1 ms in vitro, the 100-ms bursts may reflect interactions between the labeled DNA and other molecules in vivo. Although *E. coli* cells are small and
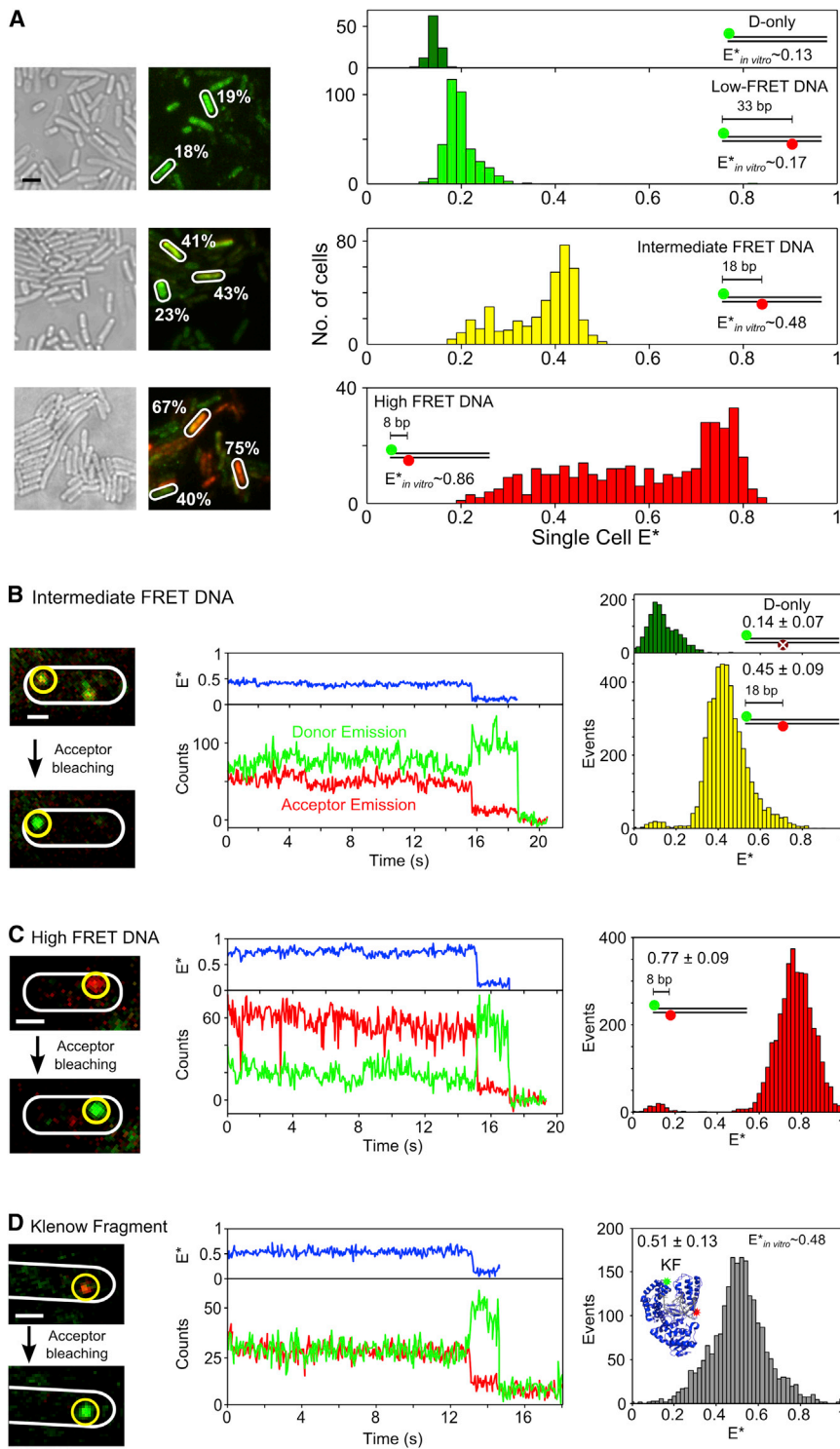
FIGURE 5 Ensemble and smFRET studies in single bacteria. (A) Analysis of cells loaded with 20 pmol each of three DNA FRET standards exhibiting low (~0.17), intermediate (~0.48), and high (~0.86) FRET (as measured using in vitro single-molecule measurements; Fig. S5 A). Left: WL and green/red (FRET) fluorescence overlay images (Scale bar: 3 μm). Examples of FRET values from different cells are indicated (white). Right (top to bottom): uncorrected cell-based FRET (E*) histograms for donor only (dark green), low (light green), intermediate (yellow), and high (red) FRET DNA standards. (B–D) In vivo smFRET. Cells loaded with 0.25 pmol intermediate-FRET DNA (panel B), 0.25 pmol high-FRET DNA (panel C), and 5 pmol doubly-labeled KF (panel D). Left column: green/red fluorescence overlay of single frame before and after acceptor photobleaching. Middle column: time traces corresponding to the molecule in the yellow circle. FRET efficiencies, donor emission intensities, and acceptor emission intensities in blue, green, and red, respectively. Right column: FRET histograms of donor only molecules (green) and donor-acceptor molecules (yellow, red, and gray) from 20 time traces for each sample. Scale bars: 3 μm for A, 1 μm for B–D.

must contain only a few molecules ($N < 10$) for single-molecule confocal detection, we were able to obtain hundreds of fluorescence bursts from single cells by treating them with the cell-wall inhibitor cephalexin, which causes cells to grow up to 100 times their normal length without dividing (63,64). Using ALEX spectroscopy to detect doubly-labeled DNAs in elongated E. coli (Fig. S7, E–G), we measured both FRET and fluorophore stoichiometry of DNAs, and distinguish them from singly-labeled species. Confocal detection provides another option for in vivo single-molecule fluorescence and FRET, particularly for rapidly diffusing molecules.

Compatibility with other organisms: fluorescent DNA and proteins in yeast

To test whether electroporation can deliver fluorescent biomolecules into other microorganisms such as yeast (as done using unmodified DNA), we electroporated *S. cerevisiae* with labeled DNA or proteins (CAP, KF). All biomolecules were successfully internalized, with most cells showing high fluorescence (Fig. S8, *left*) compared to empty cells and nonelectroporated controls (Fig. S8, *right*). Nonelectroporated cells, which have been incubated with the same amount of labeled molecules, exhibit background fluorescence as low as empty cells (autofluorescence) demonstrating that internalization of labeled molecules is a direct result of electroporation. As with electroporated *E. coli*, the loading efficiency varied between cells. The localization of the different biomolecules also exhibited different patterns (Fig. S8). These results established the high efficiency of internalization of labeled proteins and DNAs into yeast, creating prospects for extensions to other genetically diverse microorganisms.

DISCUSSION

By adapting electroporation, we developed a facile, efficient, and high-throughput method for delivering labeled biomolecules (DNA and proteins) into live *E. coli*. We characterized the copy number, mobility, and photostability of internalized labeled DNAs and proteins, and demonstrated both their structural integrity (using FRET) and functionality. Our methods add a powerful tool to the single-molecule toolbox.

OFPs are an excellent complement to FP fusions. Their brightness and photostability inside living bacteria (aided by the reducing environment of the cytoplasm) allow single-molecule monitoring for minutes, much longer than for typical FPs. Our method also allows important characterization of photophysical behavior of such constructs in vivo. Because OFPs require no maturation, they can be observed in living bacteria ~15 min after electroporation. The small size of organic fluorophores enables experiments on small proteins and peptides inaccessible with FPs, and permits facile internal labeling, crucial for intramolecular FRET studies. Intracellular smFRET offers a tractable path for single-molecule structural biology in vivo, and a unique way to visualize how protein conformational changes affect cellular mechanisms.

As with most single-molecule fluorescence work in small cells such as *E. coli*, copy-number control is important and can be achieved either by electroporating small amounts of biomolecule and selection of cells with few fluorescent molecules (up to ~5), or reaching low concentrations through bleaching. Depending on the copy number of an endogenous protein (N_{endo}), internalized proteins (with a copy number of N_{elec}) may either simply represent the endogenous pool (when $N_{endo} \gg N_{elec}$), or substantially contribute to it (when $N_{endo} \sim N_{elec}$ or $N_{endo} \ll N_{elec}$). In some cases a protein encoding gene can even be deleted from the chromosome to ensure that only internalized proteins are present. In others, the observation of a subpool of labeled proteins competing with the endogenous copies can lead to interesting competition experiments. For any experiment, it is important to determine the ratio of internalized versus endogenous copy number and this method provides a tool to control this ratio. In vivo photoswitching (as in mammalian cells (29)) can also control the number of fluorescent molecules, enabling efficient acquisition of single-molecule data, and super-resolution imaging (5–7).

In general, electroporation is compatible with many cell types, as well as chemical groups (fluorophores, unnatural nucleotides and amino acids, metal chelators, cross-linkers, caging groups), transplanting the flexibility of in vitro bioconjugation into living cells and opening new avenues for exploring cellular processes in vivo.

SUPPORTING MATERIAL

REFERENCES

1. Yildiz, A., J. N. Forkey, …, P. R. Selvin. 2003. Myosin V walks hand-over-hand: single fluorophore imaging with 1.5-nm localization. *Science.* 300:2061–2065.

2. Yu, J., J. Xiao, …, X. S. Xie. 2006. Probing gene expression in live cells, one protein molecule at a time. *Science.* 311:1600–1603.

3. English, B. P., V. Hauryliuk, …, J. Elf. 2011. Single-molecule investigations of the stringent response machinery in living bacterial cells. *Proc. Natl. Acad. Sci. USA.* 108:E365–E373.

4. Ha, T., T. Enderle, …, S. Weiss. 1996. Probing the interaction between two single molecules: fluorescence resonance energy transfer between a single donor and a single acceptor. *Proc. Natl. Acad. Sci. USA.* 93:6264–6268.

5. Betzig, E., G. H. Patterson, …, H. F. Hess. 2006. Imaging intracellular fluorescent proteins at nanometer resolution. *Science.* 313:1642–1645.

6. Hess, S. T., T. P. Girirajan, and M. D. Mason. 2006. Ultra-high resolution imaging by fluorescence photoactivation localization microscopy. *Biophys. J.* 91:4258–4272.

7. Rust, M. J., M. Bates, and X. Zhuang. 2006. Sub-diffraction-limit imaging by stochastic optical reconstruction microscopy (STORM). *Nat. Methods.* 3:793–795.

8. Heilemann, M., S. van de Linde, …, M. Sauer. 2008. Subdiffraction-resolution fluorescence imaging with conventional fluorescent probes. *Angew. Chem. Int. Ed. Engl.* 47:6172–6176.

9. Badrinarayanan, A., R. Reyes-Lamothe, …, D. J. Sherratt. 2012. In vivo architecture and action of bacterial structural maintenance of chromosome proteins. *Science.* 338:528–531.

10. Leake, M. C., J. H. Chandler, …, J. P. Armitage. 2006. Stoichiometry and turnover in single, functioning membrane protein complexes. *Nature.* 443:355–358.

11. Reyes-Lamothe, R., D. J. Sherratt, and M. C. Leake. 2010. Stoichiometry and architecture of active DNA replication machinery in *Escherichia coli. Science.* 328:498–501.

12. Taniguchi, Y., P. J. Choi, …, X. S. Xie. 2010. Quantifying *E. coli* proteome and transcriptome with single-molecule sensitivity in single cells. *Science.* 329:533–538.

13. Xie, X. S., P. J. Choi, …, G. Lia. 2008. Single-molecule approach to molecular biology in living bacterial cells. *Annu. Rev. Biophys.* 37:417–444.

14. Xie, X. S., J. Yu, and W. Y. Yang. 2006. Living cells as test tubes. *Science.* 312:228–230.

15. Lew, M. D., S. F. Lee, …, W. E. Moerner. 2011. Three-dimensional superresolution colocalization of intracellular protein superstructures and the cell surface in live *Caulobacter crescentus. Proc. Natl. Acad. Sci. USA.* 108:E1102–E1110.

16. Tsien, R. Y. 1998. The green fluorescent protein. *Annu. Rev. Biochem.* 67:509–544.

17. Hammar, P., P. Leroy, …, J. Elf. 2012. The lac repressor displays facilitated diffusion in living cells. *Science.* 336:1595–1598.

18. Miesenböck, G., D. A. De Angelis, and J. E. Rothman. 1998. Visualizing secretion and synaptic transmission with pH-sensitive green fluorescent proteins. *Nature.* 394:192–195.

19. Elowitz, M. B., A. J. Levine, …, P. S. Swain. 2002. Stochastic gene expression in a single cell. *Science.* 297:1183–1186.

20. Wang, W., G. W. Li, …, X. Zhuang. 2011. Chromosome organization by a nucleoid-associated protein in live bacteria. *Science.* 333:1445–1449.

21. Beach, D. L., E. D. Salmon, and K. Bloom. 1999. Localization and anchoring of mRNA in budding yeast. *Curr. Biol.* 9:569–578.

22. Dempsey, G. T., J. C. Vaughan, …, X. Zhuang. 2011. Evaluation of fluorophores for optimal performance in localization-based super-resolution imaging. *Nat. Methods.* 8:1027–1036.

23. Shaner, N. C., P. A. Steinbach, and R. Y. Tsien. 2005. A guide to choosing fluorescent proteins. *Nat. Methods.* 2:905–909.

24. Ponsioen, B., J. Zhao, …, K. Jalink. 2004. Detecting cAMP-induced Epac activation by fluorescence resonance energy transfer: Epac as a novel cAMP indicator. *EMBO Rep.* 5:1176–1180.

25. Landgraf, D., B. Okumus, …, J. Paulsson. 2012. Segregation of molecules at cell division reveals native protein localization. *Nat. Methods.* 9:480–482.

26. Jones, S. A., S. H. Shim, …, X. W. Zhuang. 2011. Fast, three-dimensional super-resolution imaging of live cells. *Nat. Methods.* 8:499–508.

27. Hinner, M. J., and K. Johnsson. 2010. How to obtain labeled proteins and what to do with them. *Curr. Opin. Biotechnol.* 21:766–776.

28. Keppler, A., S. Gendreizig, …, K. Johnsson. 2003. A general method for the covalent labeling of fusion proteins with small molecules in vivo. *Nat. Biotechnol.* 21:86–89.

29. Wombacher, R., M. Heidbreder, …, M. Sauer. 2010. Live-cell super-resolution imaging with trimethoprim conjugates. *Nat. Methods.* 7:717–719.

30. Zhang, Z., B. A. Smith, …, P. G. Schultz. 2003. A new strategy for the site-specific modification of proteins in vivo. *Biochemistry.* 42:6735–6746.

31. McNeil, P. L., R. F. Murphy, …, D. L. Taylor. 1984. A method for incorporating macromolecules into adherent cells. *J. Cell Biol.* 98:1556–1564.

32. Clarke, M. S., and P. L. McNeil. 1992. Syringe loading introduces macromolecules into living mammalian cell cytosol. *J. Cell Sci.* 102:533–541.

33. Taylor, D. L., and Y. L. Wang. 1978. Molecular cytochemistry: incorporation of fluorescently labeled actin into living cells. *Proc. Natl. Acad. Sci. USA.* 75:857–861.

34. Sakon, J. J., and K. R. Weninger. 2010. Detecting the conformation of individual proteins in live cells. *Nat. Methods.* 7:203–205.

35. Riveline, D., and P. Nurse. 2009. 'Injecting' yeast. *Nat. Methods.* 6:513–514.

36. Song, Y., T. Hahn, …, W. E. Huang. 2007. Ultrasound-mediated DNA transfer for bacteria. *Nucleic Acids Res.* 35:e129.

37. Dower, W. J., J. F. Miller, and C. W. Ragsdale. 1988. High efficiency transformation of *E. coli* by high voltage electroporation. *Nucleic Acids Res.* 16:6127–6145.

38. Neumann, E., M. Schaefer-Ridder, …, P. H. Hofschneider. 1982. Gene transfer into mouse lyoma cells by electroporation in high electric fields. *EMBO J.* 1:841–845.

39. Hohlbein, J., K. Gryte, …, A. N. Kapanidis. 2010. Surfing on a new wave of single-molecule fluorescence methods. *Phys. Biol.* 7:031001.

40. Kapanidis, A. N., N. K. Lee, …, S. Weiss. 2004. Fluorescence-aided molecule sorting: analysis of structure and interactions by alternating-laser excitation of single molecules. *Proc. Natl. Acad. Sci. USA.* 101:8936–8941.

41. Uphoff, S., S. J. Holden, …, A. N. Kapanidis. 2010. Monitoring multiple distances within a single molecule using switchable FRET. *Nat. Methods.* 7:831–836.

42. Santoso, Y., C. M. Joyce, …, A. N. Kapanidis. 2010. Conformational transitions in DNA polymerase I revealed by single-molecule FRET. *Proc. Natl. Acad. Sci. USA.* 107:715–720.

43. Tokunaga, M., N. Imamoto, and K. Sakata-Sogawa. 2008. Highly inclined thin illumination enables clear single-molecule imaging in cells. *Nat. Methods.* 5:159–161.

44. Young, J. W., J. C. W. Locke, …, M. B. Elowitz. 2012. Measuring single-cell gene expression dynamics in bacteria using fluorescence time-lapse microscopy. *Nat. Protoc.* 7:80–88.

45. Messina, T. C., H. Kim, …, D. S. Talaga. 2006. Hidden Markov model analysis of multichromophore photobleaching. *J. Phys. Chem. B.* 110:16366–16376.

46. Viterbi, A. J. 1967. Error bounds for convolutional codes and an asymptotically optimum decoding algorithm. *IEEE Trans. Inf. Theory.* 13:260–269.

47. Rabiner, L. R. 1989. A tutorial on hidden Markov-models and selected applications in speech recognition. *Proc. IEEE.* 77:257–286.

48. Uphoff, S., R. Reyes-Lamothe, …, A. N. Kapanidis. 2013. Single-molecule DNA repair in live bacteria. *Proc. Natl. Acad. Sci. USA.* 110:8063–8068.

49. Holden, S. J., S. Uphoff, …, A. N. Kapanidis. 2010. Defining the limits of single-molecule FRET resolution in TIRF microscopy. *Biophys. J.* 99:3102–3111.

50. Crocker, J. C., and D. G. Grier. 1996. Methods of digital video microscopy for colloidal studies. *J. Colloid Interface Sci.* 179:298–310.

51. Michalet, X., and A. J. Berglund. 2012. Optimal diffusion coefficient estimation in single-particle tracking. *Phys. Rev. E Stat. Nonlin. Soft Matter Phys.* 85:0619161–0619164.

52. Lymperopoulos, K., R. Crawford, …, A. N. Kapanidis. 2010. Single-molecule DNA biosensors for protein and ligand detection. *Angew. Chem. Int. Ed. Engl.* 49:1316–1320.

53. Thompson, R. E., D. R. Larson, and W. W. Webb. 2002. Precise nanometer localization analysis for individual fluorescent probes. *Biophys. J.* 82:2775–2783.

54. Persson, F., M. Lindén, …, J. Elf. 2013. Extracting intracellular diffusive states and transition rates from single-molecule tracking data. *Nat. Methods.* 10:265–269.

55. Kolmakov, K., V. N. Belov, …, S. W. Hell. 2010. Red-emitting rhodamine dyes for fluorescence microscopy and nanoscopy. *Chemistry.* 16:158–166.

56. Elowitz, M. B., M. G. Surette, …, S. Leibler. 1999. Protein mobility in the cytoplasm of *Escherichia coli*. *J. Bacteriol.* 181:197–203.

57. Mullineaux, C. W., A. Nenninger, …, C. Robinson. 2006. Diffusion of green fluorescent protein in three cell environments in *Escherichia coli*. *J. Bacteriol.* 188:3442–3448.

58. Nenninger, A., G. Mastroianni, and C. W. Mullineaux. 2010. Size dependence of protein diffusion in the cytoplasm of *Escherichia coli*. *J. Bacteriol.* 192:4535–4540.

59. Busby, S., and R. H. Ebright. 1999. Transcription activation by catabolite activator protein (CAP). *J. Mol. Biol.* 293:199–213.

60. Joyce, C. M., and N. D. F. Grindley. 1983. Construction of a plasmid that overproduces the large proteolytic fragment (Klenow fragment) of DNA polymerase I of *Escherichia coli*. *Proc. Natl. Acad. Sci. USA.* 80:1830–1834.

61. Shimada, T., N. Fujita, …, A. Ishihama. 2011. Novel roles of cAMP receptor protein (CRP) in regulation of transport and metabolism of carbon sources. *PLoS ONE.* 6:e20081.

62. Lee, N. K., A. N. Kapanidis, …, S. Weiss. 2005. Accurate FRET measurements within single diffusing biomolecules using alternating-laser excitation. *Biophys. J.* 88:2939–2953.

63. Gordon, G. S., D. Sitnikov, …, A. Wright. 1997. Chromosome and low copy plasmid segregation in *E. coli*: visual evidence for distinct mechanisms. *Cell.* 90:1113–1121.

64. Rolinson, G. N. 1980. Effect of beta-lactam antibiotics on bacterial cell growth rate. *J. Gen. Microbiol.* 120:317–323.